Design Optimisation of Optically Pumped Terahertz Lasers in Stepped Quantum Wells

H N Rutt, Z -J Xin and H A Tan

Optoelectronics Research Centre, University of Southampton, Highfield, Southampton SO17 1BJ, United Kingdom

PACS: 68.65.Fg, 42.60.-v, 42.60.By, 42.72.Ai

Abstract

Asymmetric stepped quantum wells have been used in many optoelectronic devices. This paper proposes a modulation doping position at the edge of the stepped well to minimise the potential distortion caused by the doping. As a result, parasitic potential wells are eliminated, and the sensitivity of the energy levels to dopant concentrations is substantially reduced. We also suggest a stacked design to juxtapose two quantum well slabs in order to improve the waveguide mode overlap in optically pumped terahertz lasers using the structure. The percentage of overlap between the active quantum wells layers and the laser mode increases from 9.8 % for a thinned-substrate single slab scheme to 68.4 % for the stacked double slabs with two highly doped layers acting as a plasma waveguide respectively. A diffraction integral model is established to simulate the laser cavity tolerance to possible misalignment in the stacked design. Our modelling result shows that the diffraction loss due to small (few micrometer) misalignment or difference in slabs length is negligible compared to other losses in the laser system.

1. INTRODUCTION

Asymmetric stepped quantum wells (QW) have been widely used in QW infrared (IR) photodetectors (QWIP) [1], nonlinear optics [2] and in the design of terahertz (1-10 THz or far-infrared as used in some of the references) lasers [3-8]. In the optically pumped terahertz lasers, asymmetric stepped QWs are used to form energy levels (or subbands), so that the lasers can operate on a three-level scheme analogous to terahertz gas lasers. The feasibility and gain threshold on these designs have been reported [6, 8]. Our previous calculation showed that the stepped wells structure as a terahertz laser offers a lower pump power threshold as compared to the coupled wells

structure [8]. The purpose of adopting an asymmetric design is to relax the quantum selection rule, in order that the electrons in the ground level can be optically pumped to the second excited level, which otherwise is not allowed. From this excited subband, electrons can transit partly to the first excited subband and partly to the ground state by non-radiative as well as radiative transitions. Therefore a two dimensional electron gas (2DEG) must be confined in the ground subband to perform the pump-relaxation cycle. This is realised by modulation doping in the QW structures. The first part of this paper will discuss the effect of modulation doping positions on the subband formation and suggest an ideal position for it, which eliminates parasitic potential wells and reduces energy level sensitivity to dopant concentrations. Veliadis et al. [9] have discussed the effects of doping position for coupled wells structures but to our knowledge, the effects on stepped wells structures have not been discussed elsewhere.

A typical period for an asymmetric QW layer used in terahertz lasers is about 60 nm. This includes a barrier of about 35 nm. Because the wavefunctions concerned are mainly confined in the width of the QW, as will be seen later in Figure 1, 2 and 4, the overlap integrals of the wavefunctions for the transition matrix thus mainly take place in this region and the effective thickness is therefore defined by the QW. This is very thin compared with the laser operation wavelengths, so the mode overlaps is poor. Although mode overlap can be improved by growing multiple QWs (MQW) up to a hundred periods, the larger thickness become impractical because of cost, morphology and uniformity constraints as discussed in [10]. The second part of this paper proposes a novel method to improve the mode overlap.

In 1989, S. I. Borenstain and J. Katz [3] first studied the feasibility of far-infrared (FIR) lasers based on intersubband transitions in QWs. There have been

many proposed optically pumped designs [4-8, 11, 12] to develop the idea. Among them the stepped QW structure [6-8] and the 'fountain' structure [11, 12] are most representative. The former is designed to work in the terahertz region above the resonant wavelength (34.4 μm) of the polarized longitudinal optical (LO) phonons, while the latter is targeted in the FIR region (10-30 μm, called 'FIR' here to distinguish it from the terahertz devices working in the 40-300 μm region) below that wavelength.

2. MODULATION DOPING IN A STEP QUANTUM WELL

In order to form a 2DEG in a stepped QW, there are three positions available for doping as shown in Figure 1, namely A, B and C. The energy levels in Figure 1 are drawn assuming low doping levels and thus negligible distortion of the band structure by the dopant.

Conventionally dopants are located at the middle of barriers at position A (so called modulation doping). For low doping levels this ensures complete ionisation of dopants at room temperature and formation of a 2DEG in the lower well by electron diffusion. However this design also has the strongest impact on the potential bottom of the conduction band, as the space charge from the ionised dopants creates an electric field between the 2DEG and itself, which is proportional to the sheet density of the space charge as described by the case in a parallel-plane capacitor. In other words, the space charge potential created is proportional to the effective distance between the doping region and the 2DEG. This added potential subsequently distorts the profile of the conduction band bottom and consequently the subband levels. If the doping becomes heavier, potential valleys can be created in the step well and the barrier, whilst 2DEGs can be confined there. In practice this leads to a coupling between the energy levels and the degree of doping which is highly undesirable from

a process control point of view. Figure 2 shows the band structure after doping in the middle of 35 nm wide barriers with a moderate concentration of 1×10^{18} cm^{-3} (other structure parameters are as shown in Figure 2) in multiple GaAs/AlGaAs QWs. The doping width is 6.8 nm. The resulting sheet density in the examples here are comparable with those used in optically pumped intersubband lasers [7, 13, 14]. The optical gain in optically pumped intersubband lasers is proportional to the carrier sheet density where a high value is desirable. As can be seen the energy levels are already severely perturbed at this doping level, and (depending on the operating temperature) the potential valleys at A and B may also trap electrons.

It is also possible to dope the lower well at position C [1]. In this case the ionised electrons have the least effect on the conduction band, as the ionised carriers are localized at their doping position. Figure 1 gives the band structure for this case. Nevertheless, the rate of ionisation will be crucially dependent on temperature since the energy level of the dopants is below the ground subband. Figure 3 self-consistently calculates the temperature dependence of electron sheet density and the Fermi level with reference to the ground subband. The data used in it is as listed in Figure 1.

Alternatively, we propose in our design to dope at position B, at the edge of the step well close to the lower well. At this position, because the doping energy level is well above the Fermi level even for heavy doping, complete ionisation of the dopants is guaranteed. Further, because it is close to the lower well, this design has a much smaller space charge potential imposed on the conduction band bottom of the QW structure. Hence it has smaller conduction band distortion and so it is technically more controllable when the structure is grown. Figure 4 simulates this case. All the parameters used in Figure 4 are the same as those in Figure 2 aside from the dopant

positioning. No "parasitic" well is produced in the barriers, and that induced in the step is both shallow and has a very thin barrier. Table 1 compares the changes of subband gaps ΔE_{21} and ΔE_{20} caused by dopant concentration fluctuation of ±10% in the two cases described in Figure 2 and 4. It is evident that for a plus or minus 10% variation of doping concentration, the gap changes are much greater for doping at A than for doping at B. In other words, the tolerance to doping fluctuation for doping at B is much higher than that for doping at A.

Overall, the sensitivity of the terahertz laser transition energy E_{21} to dopant level fluctuations is substantially reduced by a factor of 3.3, whilst the pump transition sensitivity is marginally reduced by a factor of 1.3. The unconventional placement of the dopant at the step edge thus brings two significant advantages; elimination of parasitic wells, and reduced sensitivity to dopant level errors, especially for the laser transition, whilst retaining full dopant ionisation at low temperatures.

3. MODE OVERLAP WITH THE QWS

Mode overlap is a fundamental problem in optically pumped QW terahertz lasers [8, 15]. Firstly, there is a huge difference between the pump and laser wavelengths. The former is normally a CO_2 laser at 10.6 μm; while the latter can operate anywhere between 40 and 300 μm. This makes it very difficult to obtain good overlaps between both the pump and laser modes with the active layer of the laser when they operate in a single mode as is desirable. Secondly, due to considerations of morphology and uniformity [10] and the cost of wafer growth, QW structures grown by the MBE (molecular beam epitaxy) technique are normally limited to an epitaxial thickness of about 10 μm as compared to a 350 μm thick substrate. Hence the overlaps of both the wavelengths with the active layer will inevitably be low unless some method of

confinement is used. Thirdly, the epi-layer is of course always on the surface. This makes the mode overlap even poorer. Although thinning the substrate can mitigate the second and third difficulties, the mechanical strength and handling of the laser device will deteriorate. In summary, a key issue for a single slab device is its poor mode overlap due to a thin and superficial QW layer in the slab. The active layer is severely displaced from the mode peak intensity.

Here we propose a novel design, which mechanically overlays a laser slab on another identical slab such that the QW sides of the two laser slabs are facing each other. The layout is illustrated schematically in Figure 5, showing the pump excitation and the lasing emission directions. A CO_2 laser excites the shorter side of the two samples. Terahertz emission is perpendicular to the pump beam, but concentrated at the front edge of the MQW samples near the pump side, as the gain is the highest there. Such a mechanical juxtaposition is only feasible because no electrical currents are required to flow across the mechanical boundary, and any gaps caused by irregularities on the surfaces will be far smaller than the CO_2 laser and far infrared wavelengths involved, and thus optically negligible. Consequently the QW layers are moved to the centre of the two stacked slabs and the thickness of the active layer is doubled. This overcomes the previous drawbacks with a single slab. The two slabs can be held together mechanically or, for example by free bonding. The waveguide can be realized by growing a doping layer on top of the substrate but under the buffer and MQW layers. In this case the pump and laser modes overlap can be greatly improved as can be seen in Figure 6. The refractive indexes in the QW layers are their average values [16, 17] for those wavelengths as the thickness of each individual QW layer is much less than the pump or laser wavelength. Refractive index values in the doped layers are calculated by use of the standard plasmon and phonon oscillator

model [3]. The doping concentration for the layer acting as plasmon confinement is optimised at 3×10^{17} cm^{-3} for the laser wavelength. If a heavier doping is used, then the structure will suffer a stronger loss although indeed a small fraction of overlap can be gained. This loss mainly results from free carrier absorption and it is proportional to λ^2. M. Rochat et al. [18] recently measured the loss in a similar structure but with much heavier doping (5×10^{18} cm^{-3}) and obtained a loss of 182±90 dB/cm. Taking into consideration the doping factor, it is comparable with the calculated result here of 69.0 dB/cm. For effective guiding, the doped layers should be at least 2 μm thick. Without the waveguiding effect provided by the doped layers, the overlap between the QW active layers and laser modes is very poor, in the order of a few percent. However, this scheme has an advantage that the free carrier loss is much smaller as a result of the absence of the doped layers, calculated to be 35.4 dB/cm.

Alternatively, as we mentioned in the first paragraph in Section 3, thinning the substrate of the MQW slabs can also improve the laser mode overlap with the active layer. As shown later in Table 2, we can achieve an improvement of about three times in the ratio of laser mode overlap for the terahertz TE_0 mode by stacking the thinned slabs. Note that the pump mode overlap remains small in this case since the pump mode is not very well guided. We have found that the pump mode has a sharp dip near the centre (where the MQW layers are situated), which results in the small overlap value.

In practice, a wafer is cleaved into strips and then into slabs, so the two slabs used in a laser device are from the same strip and of the same width. However it is possible to misalign the two slabs axially when mounting them. If this happens at the two facets acting as cavity mirrors transverse to the pump direction, it will naturally result in phase shift from the two misaligned reflecting facets and consequently have

an adverse effect on the mode diffraction loss. For the pump the misalignment in the pump direction is unimportant, as the pump beam is not resonated. In the following section we estimate the tolerance to this cavity misalignment. This form of cavity, laterally split into two parts of equal length but displaced with respect to each other, has not previously been analysed to our knowledge. The loss sensitivity to the axial displacement is a critical issue with regard to its practicality.

4. CAVITY MODELING

1.1 Diffraction Integral Model

We have employed the diffraction integral method pioneered by Fox and Li [19] to determine the lowest order transverse modes in Fabry-Perot interferometers [20, 21]. The diffraction integral is modified for our resonator system. This system is modelled to determine the possible diffraction loss due to the misalignments for the optical pumping scheme proposed here. Note that this calculation is only valid for the stacked slabs without doped layers in their substrates. Briefly, the model assumes a transverse electromagnetic field distribution, which is propagated back and forth between the two end mirrors. We have performed a one-dimensional calculation only as the system is effectively infinite in the second transverse plane. This approach is appropriate since in the transverse direction at the end mirrors there is very likely to be a step change due to either the two samples not perfectly aligned or the two samples having slightly different lengths. Either of these two scenarios will result in a phase jump in the wave front on reflection.

The calculation is valid for mirror dimensions, which are large compared to the wavelength and also satisfy the condition

$$N_0 = a^2 n / L\lambda << (L/a)^2 \qquad (1)$$

where N_0 is the Fresnel number, a is the mirror height (the thickness of a MQW sample in our case), n the refractive index of the cavity medium, L the cavity length and λ is the wavelength of the electromagnetic wave.

As shown in Figure 7, integration over the dimension of the end mirrors will encounter a step discontinuity at x=0. This will result in a step change in the optical path between the two points of reference. We have denoted the length by which the two samples are misaligned by s, whereas ΔL is the difference in length between the two samples. Note that ΔL is positive (negative) if the upper sample is shorter (longer) than the lower sample. The optical path r between two points of the opposite mirrors is calculated from the x positions of the two points.

Suppose an arbitrary wave function U_q, where subscript q refers to the transit number of the wave propagation between the two mirrors, is launched at the left hand side of the cavity. We obtain for the forward transition from the left to the right, the corresponding wave function U_{q+1} at the right hand side of the cavity as

$$U_{q+1}(x_2) = \frac{\exp(j\pi/4)}{\sqrt{\lambda}} \cdot C_1 \cdot \int_{-a}^{0} U_q(x_1) \exp\left(-jk \cdot C_2 \cdot [x_1 - x_2]^2\right) dx_1 + \frac{\exp(j\pi/4)}{\sqrt{\lambda}} \cdot C_3 \cdot \int_{0}^{+a} U_q(x_1) \exp\left(-jk \cdot C_4 \cdot [x_1 - x_2]^2\right) dx_1 \quad (2)$$

where $C_1 = \exp(-jkL)/L$, $C_2 = 1/2L$, $C_3 = \exp(-jk[L+s])/(L+s)$ and $C_4 = (L+s)/2L^2$ for $-a < x_2 < 0$ while $C_1 = \exp(-jk[L-\Delta L-s])/[L-\Delta L-s]$, $C_2 = (L-\Delta L-s)/2(L-\Delta L)^2$, $C_3 = \exp(-jk[L-\Delta L])/(L-\Delta L)$ and $C_4 = 1/2(L-\Delta L)$ for $0 < x_2 < +a$. $k = 2n\pi/\lambda$ is the propagation constant of the medium between the two end mirrors.

Similarly, the subsequent wave function after a complete round trip U_{q+2} for the backward transition from the right to the left of the cavity is given by the following equation:

$$U_{q+2}(x_1) = \frac{\exp(j\pi/4)}{\sqrt{\lambda}} \cdot C_5 \cdot \int_{-a}^{0} U_{q+1}(x_2) \exp\left(-jk \cdot C_6 \cdot [x_2 - x_1]^2\right) dx_2 + \frac{\exp(j\pi/4)}{\sqrt{\lambda}} \cdot C_7 \cdot \int_{0}^{+a} U_{q+1}(x_2) \exp\left(-jk \cdot C_8 \cdot [x_2 - x_1]^2\right) dx_2 \quad (3)$$

where $C_5 = \exp(-jkL)/L$, $C_6 = 1/2L$, $C_7 = \exp(-jk[L-\Delta L-s])/(L-\Delta L)$ and $C_8 = (L-\Delta L-s)/2(L-\Delta L)^2$ for $-a < x_1 < 0$ while $C_5 = \exp(-jk[L+s])/(L+s)$, $C_6 = (L+s)/2L^2$, $C_7 = \exp(-jk[L-\Delta L])/(L-\Delta L)$ and $C_8 = 1/2(L-\Delta L)$ for $0 < x_1 < +a$.

Hence, we can iteratively compute (2) and (3), up to a number of transitions where a reasonable accuracy has been achieved for the normalized iterative amplitude after each round trip. In our case, we have plotted the diffraction power loss as a function of the roundtrip propagations to determine the level of convergence. The diffraction loss is defined as (4) in the following section.

1.2 Diffraction Loss

After many transits, the wave functions at the end mirrors have negligible change for subsequent round trip transition, except for a constant complex factor. The diffraction loss per round trip due to diffraction effects at the end mirrors can then be calculated as

$$\text{Diffraction loss per round trip} = 1 - |\gamma|^2 \quad (4)$$

where γ is the ratio U_{q+2}/U_q for an arbitrary chosen point at the mirror, $x = 0.5a$ for example.

We have used a uniform plane wave function with unity amplitude as the initial launched function U_0. The total number of transits in each calculation depends on the level of convergence of the iterative integral. Figure 8 shows some examples of the power loss as a function of the number of roundtrip propagations. The power loss for a given resonator will converge to a value after a number of back and forth

propagations, when the lowest order mode has been achieved. We have calculated the loss in less than a hundred roundtrips for cases with good convergence, whereas two hundred or more roundtrips were calculated for cases with slow convergence. Figure 8a and 8b illustrate cases with slower convergence as compared to those in Figure 8c and 8d. In particular, Figure 8b shows that the diffraction loss has yet to converge to within 0.1% of the final loss value after 200 roundtrip propagations. Note that the loss plotted in Figure 8 can only be equated to cavity loss once steady state has been reached. The oscillations, and apparent negative losses for small numbers of round trips, result from the varying intensity distribution.

Figure 9 shows the diffraction loss per round trip as a function of Fresnel number for a number of combinations of misalignment and cavity length difference. Note that the irregularities of the loss values for the top two lines at high Fresnel number are probably due to the condition in (1) has not been well satisfied. For comparison, the Fresnel reflectivity of the uncoated GaAs if used as a mirror is 33.7% at laser wavelength of 60 μm [16], so that losses substantially less than 66% are expected to have a small effect on the device threshold.

5. DISCUSSION

We have chosen our sample dimension as 2.5 mm x 1 mm x 0.3 mm where L = 1 mm. The 2.5 mm long samples are cleaved from the same strip of 1 mm wide, thus minimizing the difference between the cavity lengths in our laser system. We have calculated the loss per round trip of various cavity lengths, keeping the same value of a. However, we have not included the calculation for L = 1 mm since the conditions in (1) is not satisfied for this value of L. Nevertheless, there is sufficient evidence from our calculation results that for L = 1 mm, which correspond to N_0 = 5.1, the diffraction loss due to small (~ 4 μm) misalignment or difference in cavity lengths is

negligible compared to other losses. In addition, there are some numerical stability problems that we have encountered in this model. The model needs to avoid certain values of Fresnel Number to ensure convergence in the integral. Incorrect mode calculation may occur if the N_0 values chosen do not result in the convergence of the diffraction integral model. This numerical problem is more severe as the values of s and ΔL are increased. These calculations show that a design using stacked cleaved samples appears entirely feasible, with achievable mechanical tolerances, and brings with it the considerable advantages of much better mode overlap and an on-axis mode.

As for the case of the stacked slabs with doped layers, we can estimate the diffraction loss by considering the higher order modes loss of a reflected wave from a plane mirror with a phase step in the center. With a phase step introduced, the reflected wave consists of the fundamental mode plus the sum of all the higher order modes. Considering a symmetric mode wave function, as in our case, the electromagnetic field ratio of the fundamental modes in the reflected wave over the incident wave is given by $\cos(2n\pi s/\lambda)$. This expression is obtained assuming that the laser mode is fully confined between the doped layers of the MQW slabs. Hence, the power loss per transit due to the higher order modes is simply $1- \cos^2(2n\pi s/\lambda)$. The symbols have the same meaning as in previous paragraphs. For example, a misalignment length, s of 1 μm results in a diffraction loss per transit of 14.1 %, using the average refractive index value of 3.67 for the MQW layer at $\lambda = 60$ μm. The diffraction loss greatly increases to 48.3 % for $s = 2$ μm, suggesting an increase in sensitivity to the axial misalignment compared to the stacked slabs without heavy doped layers.

Comparing the un-thinned substrate cases, adding the doping layers greatly increases the laser mode overlap with MQW active layers by a factor of 35. On the other hand, extra losses are introduced with the doping layers, ~7-30 dB extra free carrier loss for a 1 mm cavity and extra sensitivity to misalignment related diffraction loss. Comparing the gain in overlap ratio and extra losses introduced, it appears that the doped layers scheme enhances the terahertz laser system. This scheme however has a drawback that it requires high accuracies in aligning the two laser slabs. Alternatively, by stacking two slabs after thinning the substrates; the active layers are doubled and the laser mode overlap is improved by about 3 times. Provided that the misalignment or slab length difference is practically small, the laser gain can be improved. The pump mode overlap can be increased if the total thickness of the two slabs is impractically thin. This will result in a well-confined TM_0 pump mode with high overlap ratio.

Table 2 summarizes the various pumping schemes and the corresponding design factors that we have considered in this paper. Stacking two slabs facing each other seems attractive in improving the terahertz laser gain. Thinning the substrate of the QW slabs also increases the laser mode overlap. Nevertheless, the slabs must still have a reasonable thickness such that mechanical handling is not severely constrained. Addition of the doped layers improves the waveguiding effect on the laser emission but introduce extra losses at the same time. In this case the two laser slabs have to be positioned and aligned to within micrometer accuracy, such that the resulted diffraction loss does not become comparable with other losses. Compared with the others, the staking scheme with doped layers in the substrates has the overall advantage.

6. CONCLUSION

We have discussed in this paper the doping schemes for optically pumped MQW terahertz lasers as well as a novel idea to improve the overlap between the QW active layers and the pump and laser modes. Out of the three doping scheme, we conclude that doping at the edge of the step well is a much better choice in terms of the removal of parasitic wells, sensitivity to the fluctuation of doping concentration and retention of full dopant ionisation at low temperature. We have also found that mode overlap of the terahertz laser system can be greatly improved by stacking two slabs with the MQWs side facing each other. A diffraction integral model has shown that the diffraction loss for this pumping scheme is not significant for reasonably small axial misalignments or slab length differences (~3-5 μm which is less than $\lambda/2n$). In order to increase mode overlap, heavy doped layers can be included in the MQW structures to provide the plasmon waveguiding effects. On the other hand, this gain will be offset by a fractional factor of the free carrier loss from the introduction of the doped layers. Moreover, the inclusion of doped layers has increased the diffraction loss sensitivity due to the axial misalignments or slab length difference. It is thus crucial to align and position the slabs in accuracy of the order of micrometer scale. On balance, the stacked, doped confinement design probably offers the best compromise of practicality and threshold.

Acknowledgment

The authors sincerely thank C Stanley at the University of Glasgow for very helpful discussion, which inspired the first part of the paper. This work was supported by the Engineering and Physical Sciences Research Council (EPSRC), UK.

REFERENCES

[1] Levine B F 1993 *J. Appl. Phys.* **74** R1

[2] Khurgin J B 1999 *Semiconductors and Semimetals* vol. **59** eds Garmire E and Kost A (London: Academic Press) p 1

[3] Borenstain S I and Katz J 1989 *Appl. Phys. Lett.* **55** 654

[4] Afzali-Kushaa A, Haddad G I and Norris T B 1995 *IEEE J. Quantum Electron.* **31** 135

[5] Smet J H, Fonstad C G and Hu Q 1996 *J. Appl. Phys.* **79** 9305

[6] Berger V 1994 Semicond. Sci. Technol. **9** 1493

[7] Harrison P and Kelsall R W 1997 *J. Appl. Phys.* **81** 7135

[8] Xin Z-J and Rutt H N 1997 *Semicond. Sci. Technol.* **12** 1129

[9] Veliadis J V D, Khurgin J B and Ding Y J 1996 *IEEE J. Quantum Electron.* **32** 1155

[10] Xin Z-J and Rutt H N 1998 *J. Appl. Phys.* **83** 1491

[11] Julien F H, Saar A, Wang J and Leburton J P 1995 *Electron. Lett.* **31** 838

[12] Gauthier-Lafaye O, Sauvage S, Boucaud P, Julien F H, Prazeres R, Glotin F, Ortega J-M, Thierry-Mieg V, Planel R, Leburton J-P and Berger V 1997 *Appl. Phys. Lett.* **70** 3197

[13] Kinsler P, Harrison P and Kelsall R W 1999 *J. Appl. Phys.* **85** 23

[14] Gauthier-Lafaye O, Sauvage S, Boucaud P, Julien F H, Glotin F, Prazeres R, Ortega J-M, Thierry-Mieg V and Planel R 1998 *J. Appl. Phys.* **83** 2920

[15] Singh J 1995 *Semiconductor Optoelectronics* (London: McGraw-Hill) Chapter 10

[16] Palik E D 1985 *Gallium Arsenide (GaAs)* (*Handbook of Optical Constants of Solids)* ed Palik E D (London: Academic Press) p 429-443

[17] Glembocki O J and Takarabe K 1985 *Aluminium Gallium Arsenide (AlxGa1-xAs) (Handbook of Optical Constants of Solids II)* ed Palik E D (London: Academic Press) p 513-558

[18] Rochat M, Beck M, Faist J and Oesterle U 2001 *Appl. Phys. Lett.* **78** 1967

[19] Fox A G and Li T 1961 *Bell System Technical Journal* **40** 453

[20] Yariv A 1991 *Optical Electronics* 4th edn (London: Saunders College) Chapter 4

[21] Kogelnik H and Li T 1966 *Appl. Opt.* **5** 1550

List of figures

Figure 9. Loss per round trip as a function of the Fresnel Number N_0 with $a = 0.3$ mm, $n = 3.77$ and $\lambda = 60$ μm, for various combination of s and ΔL.

List of tables

Table 1, Intersubband energy tolerance to a doping concentration fluctuation of ±10% at doping positions A and B.

	Doping at B		Doping at A	
	ΔE_{21}(meV)	ΔE_{20}(meV)	ΔE_{21}(meV)	ΔE_{20}(meV)
N_d + 10%	+0.3	-1.5	+1.0	-1.9
N_d - 10%	-0.3	+1.5	-1.1	+1.8

Table 2, Several design factors for a single slab with substrate thinned, two stacked slabs with doped layers, two stacked slabs without doped layers, as well as two stacked slabs with substrate thinned to a thickness of 15.75 μm. We have used 3 μm thick MQW layer in these calculations. The overlap value of single slab with thinned substrate is obtained using the same criteria as the two stacked slabs case. We have assumed the total thickness of the slab as 300 μm for the un-thinned cases.

[a] This is calculated as the product of mode overlap and the roundtrip transmission ratio, $\exp(-2\alpha L)$ where the chosen cavity length, L = 1 mm and α is the absorption coefficient for the sample. A higher value indicates a lower threshold for laser action.

[b] The thinned slabs are only 15.75 μm thick for each slab, which is comparable with the laser wavelength. Hence, the diffraction loss cannot be calculated here with the diffraction integral method. The misalignment tolerance is estimated to be between 1-4 μm based on the mode confinement ratio as compared to the other cases.

	Design factors	Single slab (thinned)	Stacked (not doped)	Stacked (doped)	Stacked (not doped but thinned)
i	Pump TM_0 mode overlap	0.2 %	1.9 %	80.6 %	0.2 %
ii	Laser TE_0 mode overlap	9.8 %	1.9 %	68.4 %	28.8 %
iii	Free carrier loss	34 dB/cm	35 dB/cm	69 dB/cm	26 dB/cm
iv	Transmission product of (ii) and (iii) [a]	0.02	0.004	0.03	0.09
v	Misalignment tolerance	N/A	~ 4 μm	~ 1 μm	[b]
vi	Durability	Poor	Good	Good	Poor
vii	Fabrication complexity	High	Low	Low	Very high

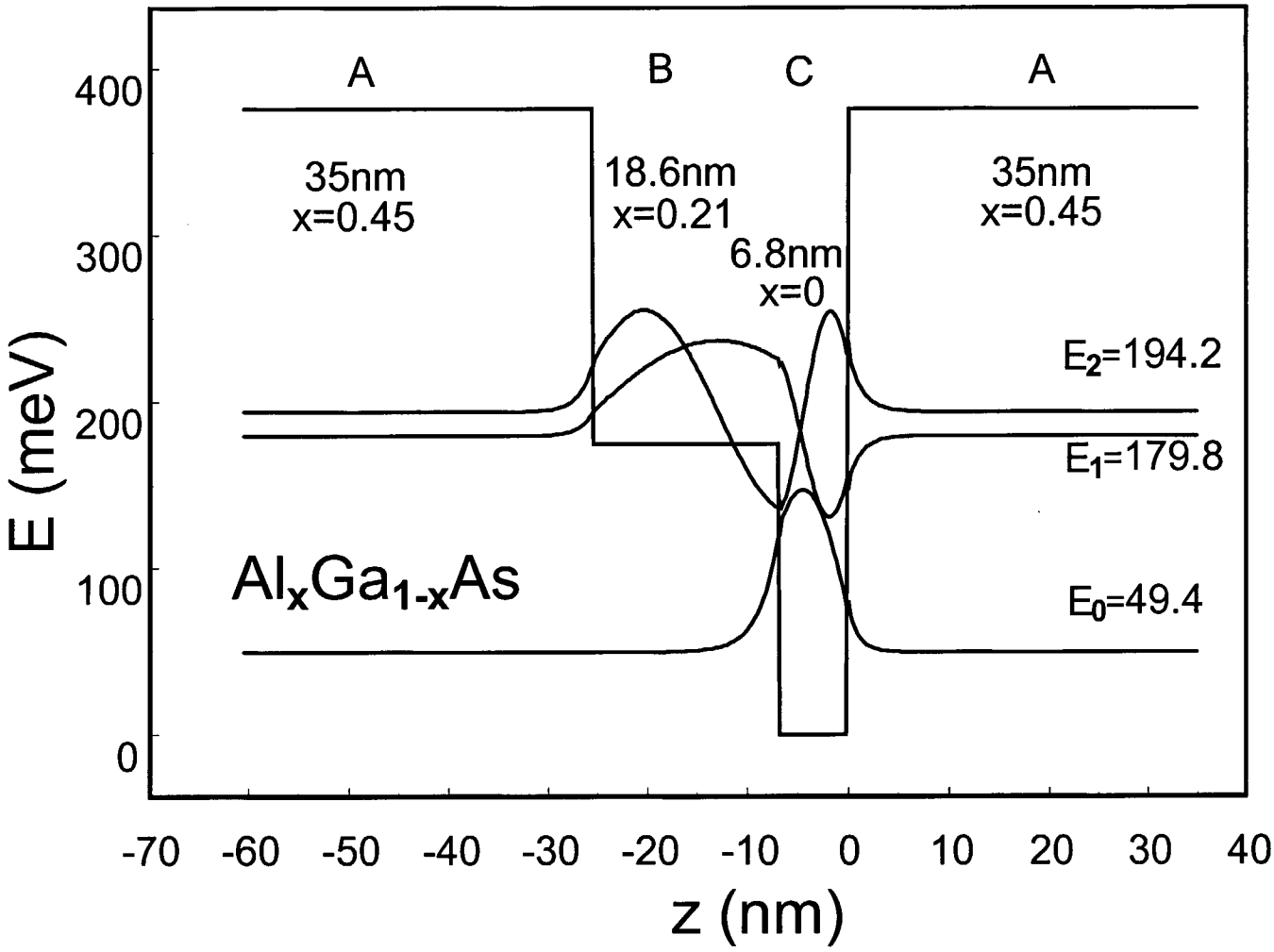
A
B
C
A
35nm
x=0.45
18.6nm
x=0.21
6.8nm
x=0
35nm
x=0.45
E_2=194.2
E_1=179.8
E_0=49.4
$Al_xGa_{1-x}As$
E (meV)
400
300
200
100
0
-70
-60
-50
-40
-30
-20
-10
0
10
20
30
40
z (nm)

Figure 1

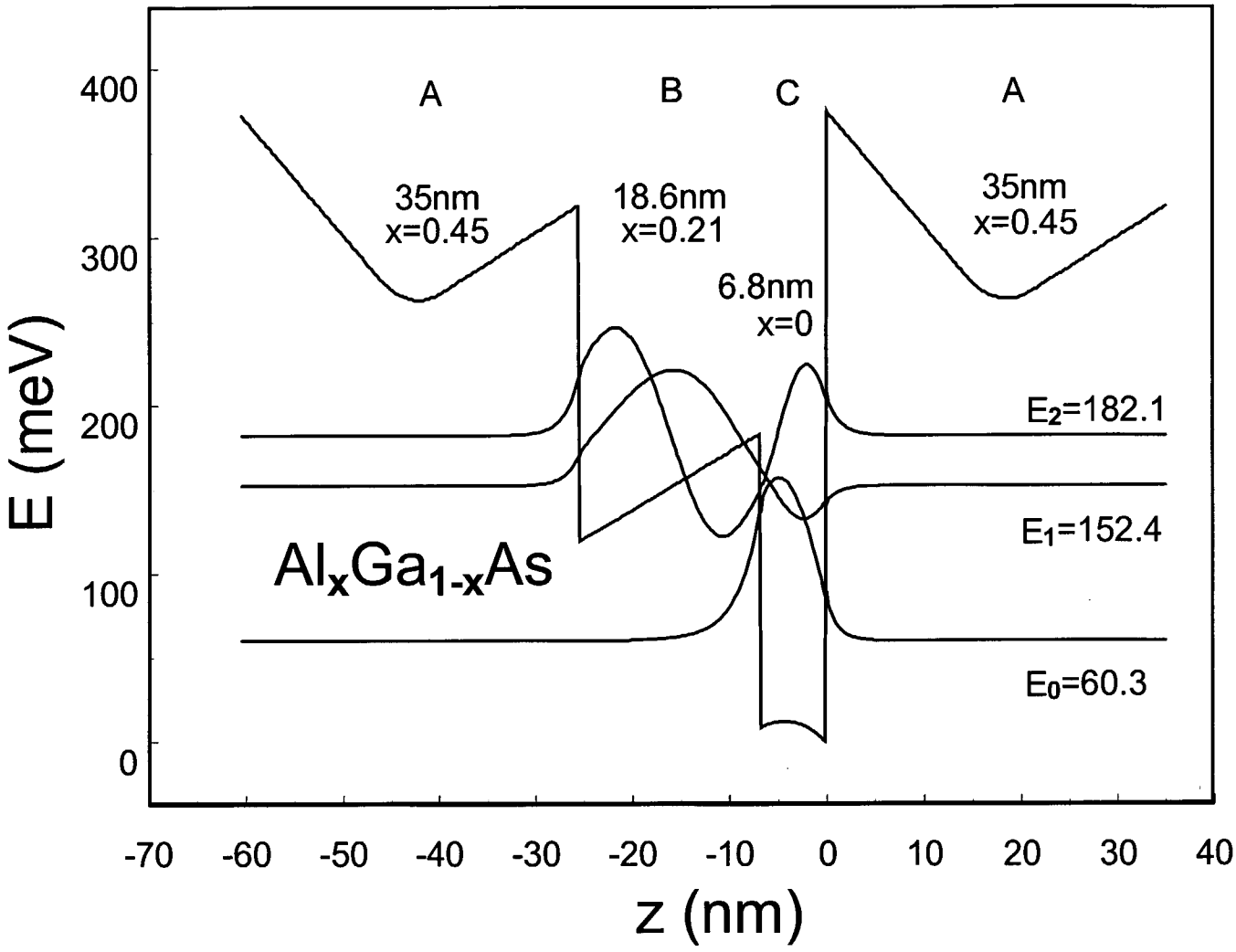
A
B
C
A
35nm
x=0.45
18.6nm
x=0.21
6.8nm
x=0
35nm
x=0.45
E2=182.1
E1=152.4
E0=60.3
AlxGa1-xAs
E (meV)
z (nm)
400
300
200
100
0
-70
-60
-50
-40
-30
-20
-10
0
10
20
30
40

Figure 2

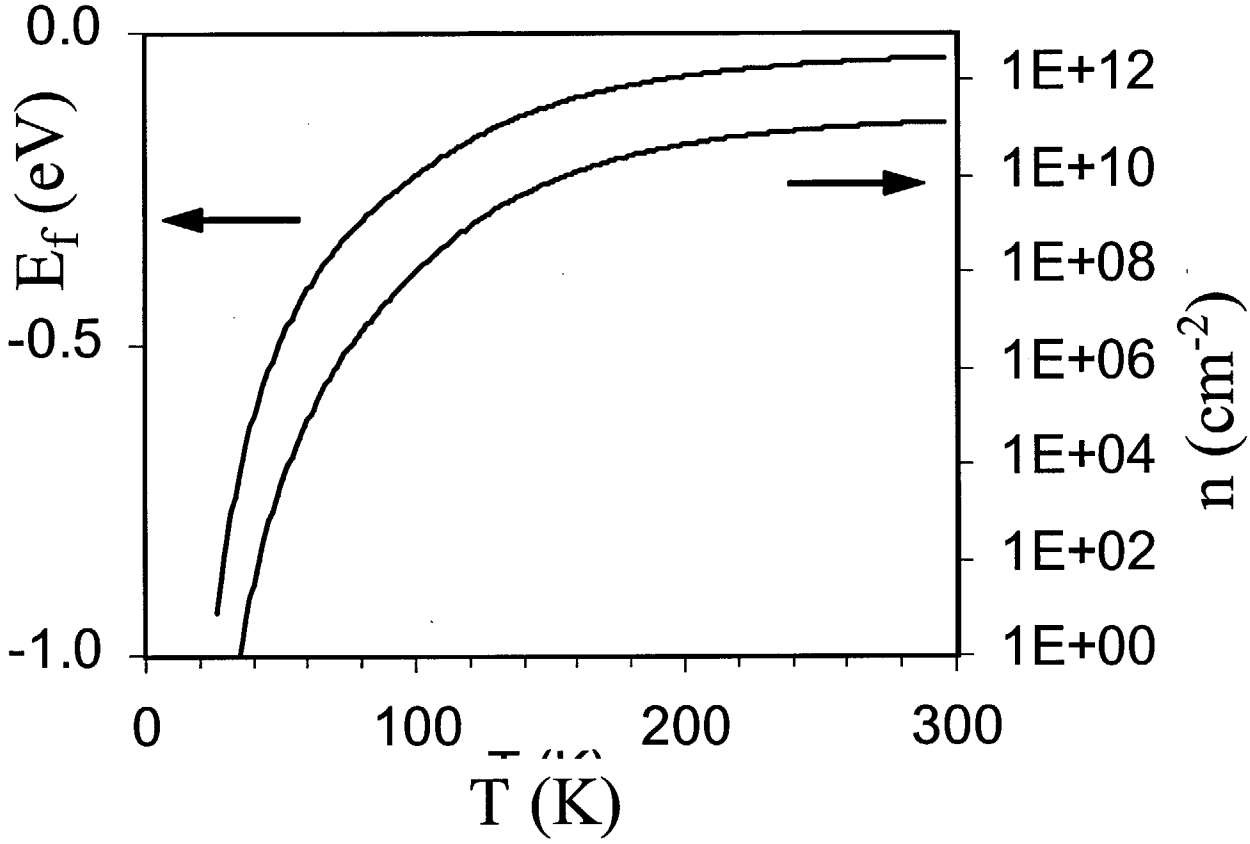
0.0
-0.5
-1.0
- E_f (eV)
1E+12
1E+10
1E+08
1E+06
1E+04
1E+02
1E+00
n (cm^{-2})
0
100
200
300
T (K)

Figure 3

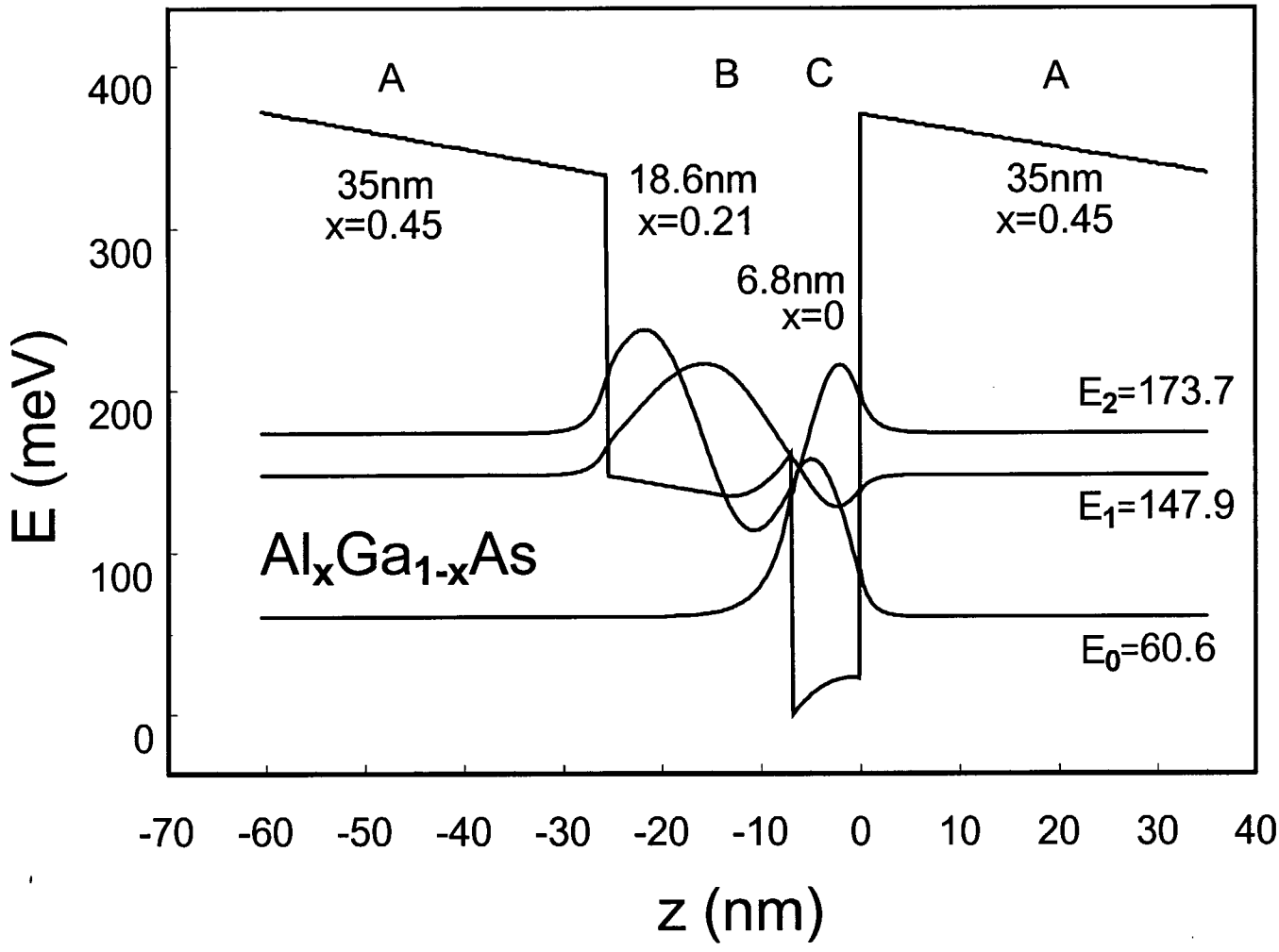
A
B
C
A
35nm
x=0.45
18.6nm
x=0.21
6.8nm
x=0
35nm
x=0.45
E_2=173.7
E_1=147.9
E_0=60.6
$Al_xGa_{1-x}As$
E (meV)
400
300
200
100
0
-70
-60
-50
-40
-30
-20
-10
0
10
20
30
40
z (nm)

Figure 4

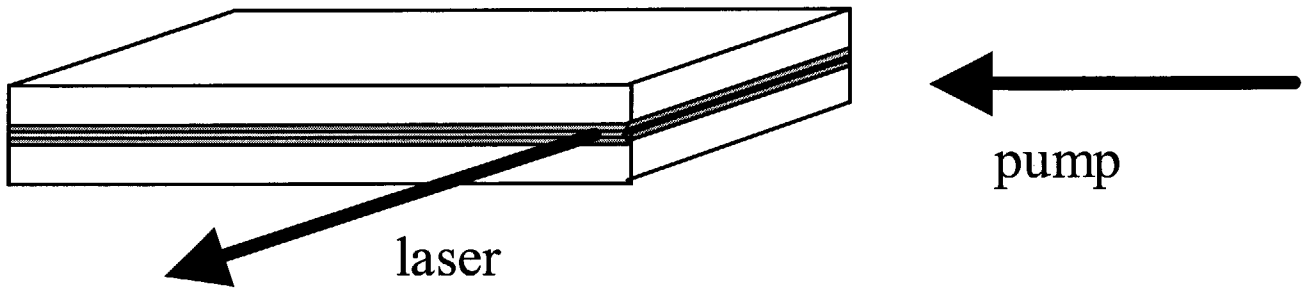

Figure 5

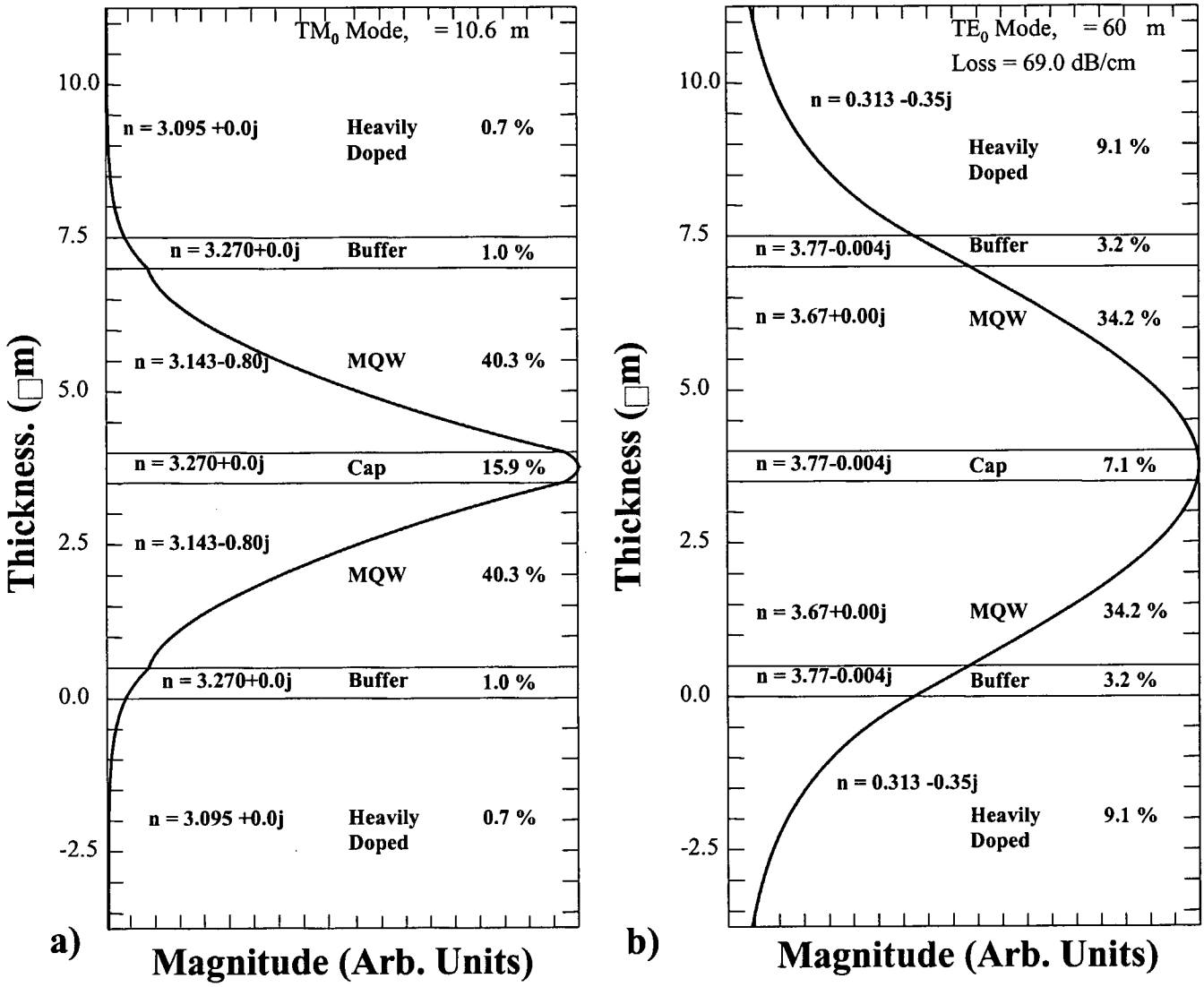
TM0 Mode, = 10.6 m
10.0
7.5
5.0
2.5
0.0
-2.5
n = 3.095 +0.0j
Heavily Doped
0.7 %
n = 3.270+0.0j
Buffer
1.0 %
n = 3.143-0.80j
MQW
40.3 %
n = 3.270+0.0j
Cap
15.9 %
n = 3.143-0.80j
MQW
40.3 %
n = 3.270+0.0j
Buffer
1.0 %
n = 3.095 +0.0j
Heavily Doped
0.7 %
Thickness. (□m)
a)
Magnitude (Arb. Units)
TE0 Mode, = 60 m
Loss = 69.0 dB/cm
10.0
7.5
5.0
2.5
0.0
-2.5
n = 0.313 -0.35j
Heavily Doped
9.1 %
n = 3.77-0.004j
Buffer
3.2 %
n = 3.67+0.00j
MQW
34.2 %
n = 3.77-0.004j
Cap
7.1 %
n = 3.67+0.00j
MQW
34.2 %
n = 3.77-0.004j
Buffer
3.2 %
n = 0.313 -0.35j
Heavily Doped
9.1 %
Thickness (□m)
b)
Magnitude (Arb. Units)

Figure 6

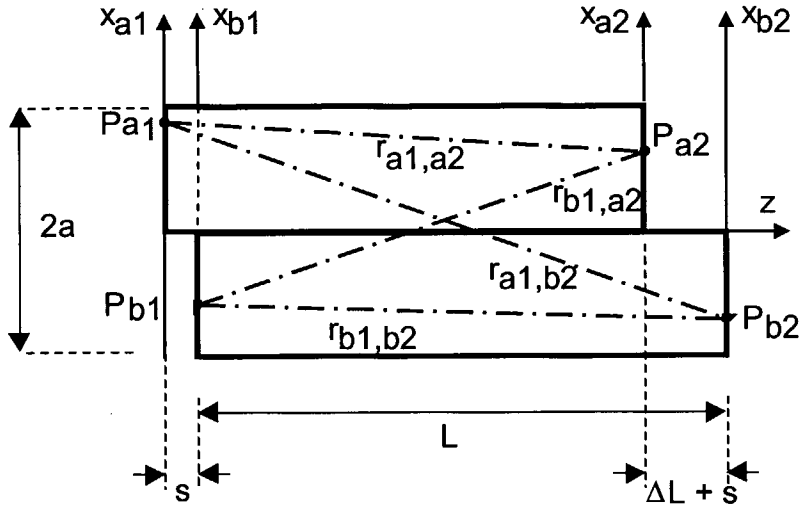
xa1
xb1
xa2
xb2
Pa1
Pa2
ra1,a2
rb1,a2
z
2a
ra1,b2
Pb1
Pb2
rb1,b2
L
s
ΔL + s

Figure 7

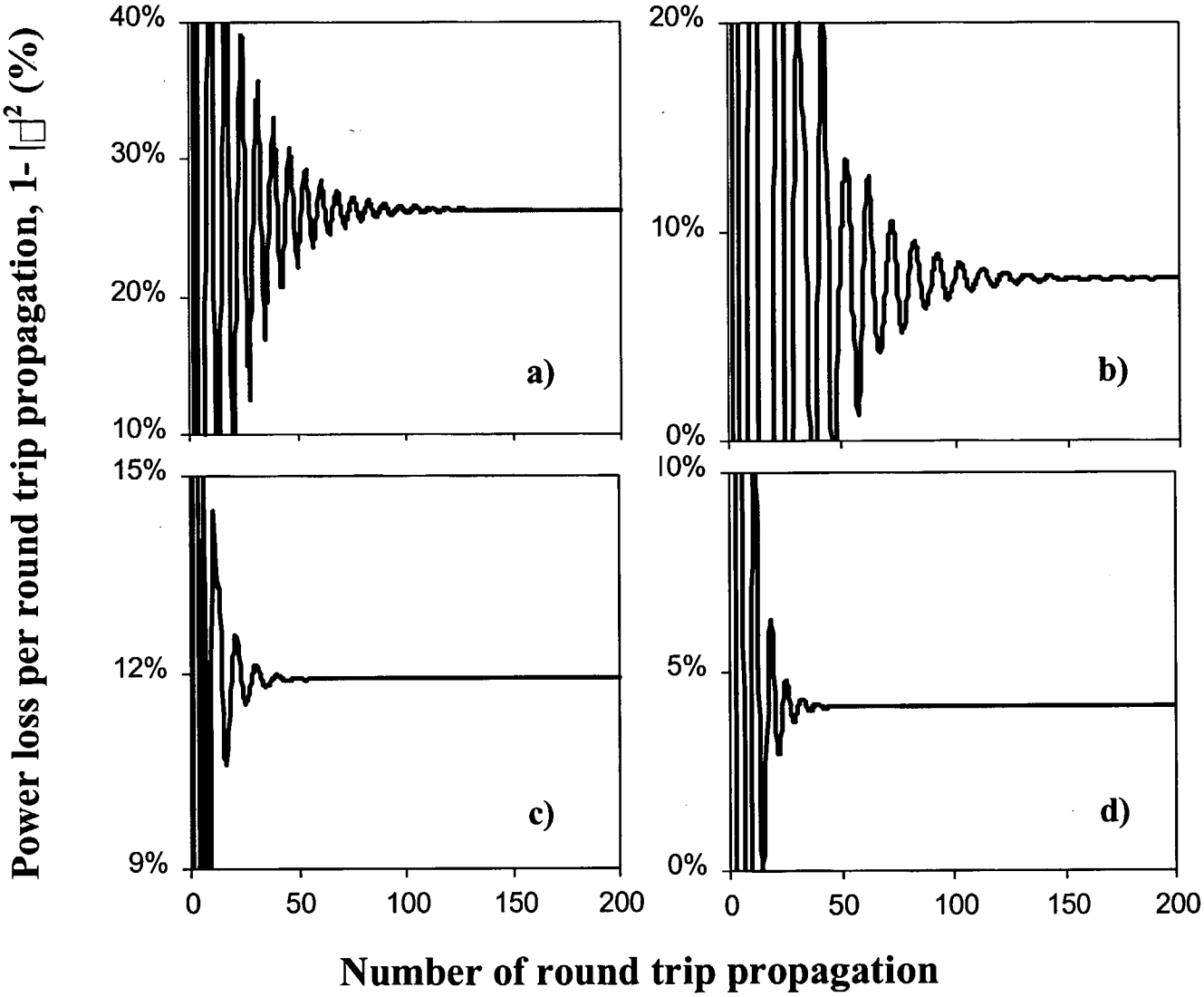
Power loss per round trip propagation, 1- |□|² (%)
40%
30%
20%
10%
a)
20%
10%
0%
b)
15%
12%
9%
c)
10%
5%
0%
d)
0
50
100
150
200
0
50
100
150
200
Number of round trip propagation

Figure 8

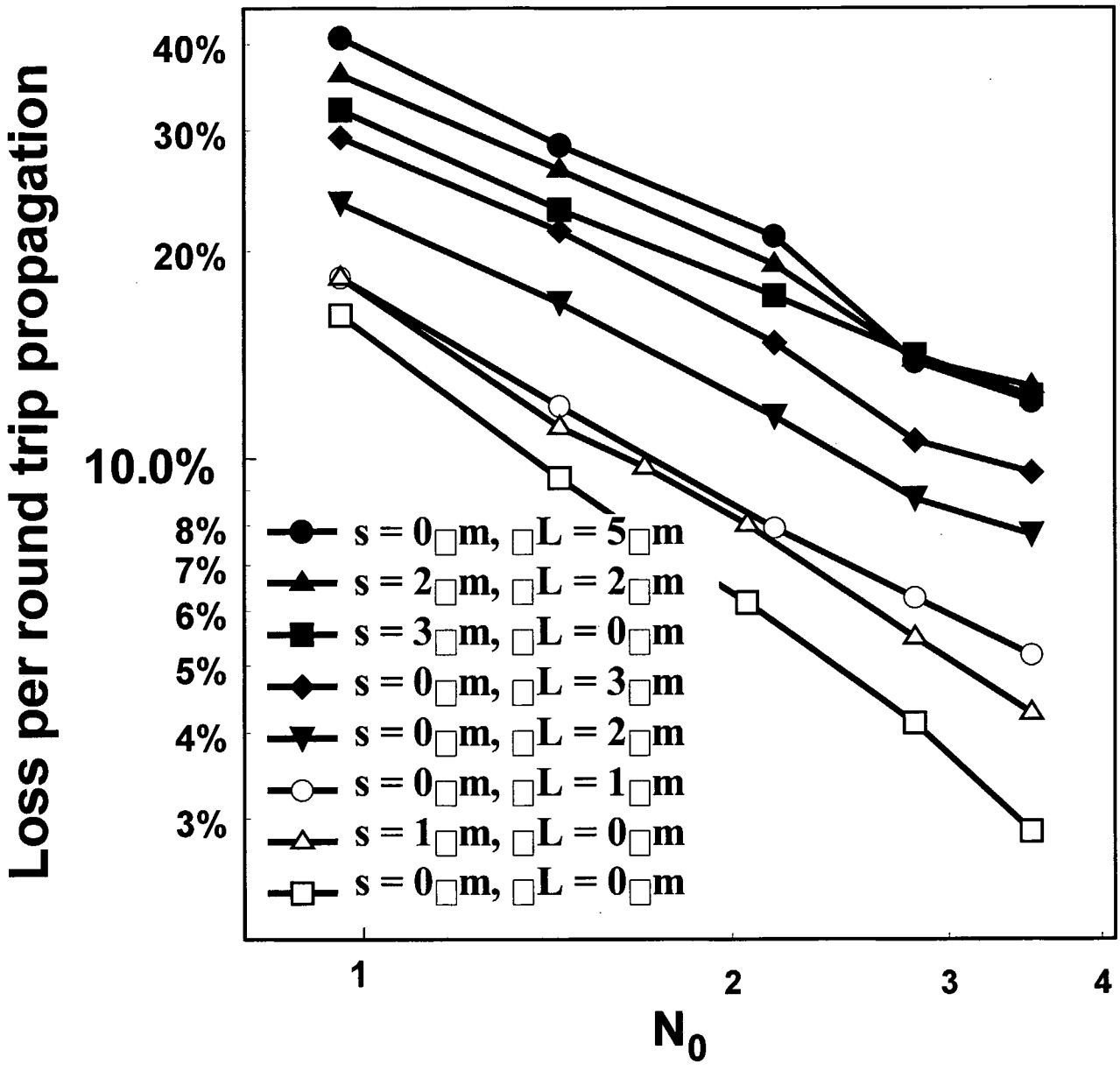
Loss per round trip propagation
40%
30%
20%
10.0%
8%
7%
6%
5%
4%
3%
s = 0□m, □L = 5□m
s = 2□m, □L = 2□m
s = 3□m, □L = 0□m
s = 0□m, □L = 3□m
s = 0□m, □L = 2□m
s = 0□m, □L = 1□m
s = 1□m, □L = 0□m
s = 0□m, □L = 0□m
1
2
3
4
N0

Figure 9